Proceedings of the 20th National Conference on Superconductivity "New Phases, Concepts and Advances"

Termination Dependence of the Surface States in Pb_2Pd

S. Basak and A. Ptok*

Institute of Nuclear Physics, Polish Academy of Sciences, W.E. Radzikowskiego 152, PL-31342 Kraków, Poland

Doi: 10.12693/APhysPolA.143.195 *e-mail: aptok@mmj.pl

The topological properties of the systems lead to the emergence of surface states that can be observed experimentally within the angle-resolved photoemission spectroscopy measurements. Recently, the topological properties of Pb_2Pd were reported. In this paper, we discuss the role of surface termination on the realized surface states. We discuss the termination dependence of the surface state for surfaces (001) and (110). We demonstrate that the Pd terminated (001) surface allows the realization of the Dirac cone-like surface state. In the case of (110), we observe clearly visible surface states with a parabolic-like dispersion relation in close vicinity of the Fermi level.

topics: ab initio, electronic properties, Fermi surface, surface states

1. Introduction

Surface states and their topological behaviors were intensively investigated in past years [1, 2]. The best example of such states can be the "metallic" surface states experimentally observed within the angle-resolved photoemission spectroscopy (ARPES) in the topological insulators [3–5]. Topological surface states preserve their properties also in the presence of magnetic impurities [6–8] and in the presence of intrinsic magnetism can be a source of new classes of magnetic topological insulators [9–12]. More recently, realizations of the Dirac [13–15], Weyl [16–20], or nodal line [21–27] semimetals have also drawn a lot of attention.

Metalic systems can also exhibit topological properties. One such example is Pb_2Pd, which was first recognized as a superconductor in 1962 [28]. XRD powder measurements confirm the realization of the $I4/mcm$ space group [29]. The system remained the same after Bi-doping, and cell volume increased monotonically with higher Bi content [30]. Similarly to $PdTe_2$ [31], Pb_2Pd exhibit conventional s-wave superconducting behavior of a specific heat jump at T_c around 3 K [28, 29, 32].

Independent of the realized symmetry, Pd-compounds (like $PdAu_2$ [33], $PdSb_2$ [34], $PdTe_2$ [35–38], or $PdBi_2$ [39, 40]) typically exhibit topological properties. For example, in the case of $PdTe_2$ (with $P\bar{3}m1$ symmetry) the bulk Dirac point and topological surface states were reported [35–38]. Preliminary theoretical results also suggest topological properties in the case of Pb_2Pd [29], however, this feature is yet to be properly studied. In this paper, we discuss the electronic properties of Pb_2Pd (electronic bulk band structure and the termination dependence of surface states), presented on Fig. 1. The paper is organized as follows. In Sect. 2, we present and discuss our numerical results, which are concluded in Sect. 3.

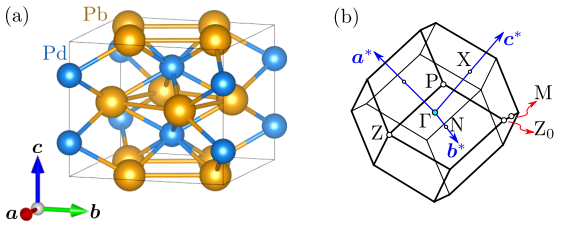

Fig. 1. Crystal structure of Pb_2Pd with $I4/mcm$ symmetry (a) and the corresponding Brillouin zone with their high symmetry points (b).

2. Numerical results and discussion

2.1. Calculation details

The first-principle calculations were performed within density-functional theory (DFT) using the projector augmented-wave (PAW) method [41] implemented in the Vienna *ab initio* simulation package (VASP) [42–44]. The exchange-correlation potential was obtained by the generalized gradient approximation (GGA) in the form proposed by Perdew, Burke, and Enzerhof (PBE) [45]. The energy cut-off for plane-wave expansion was equal

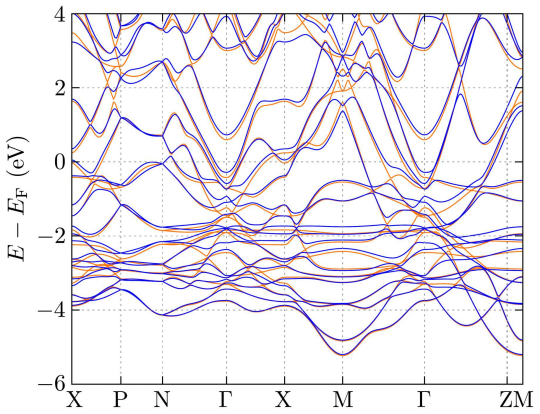

Fig. 2. Bulk electronic band structure of Pb_2Pd with $I4/mcm$ symmetry. The orange and blue line show results in the absence and presence of spin–orbit coupling, respectively.

to 400 eV. Conventional cell optimization was performed using a $12 \times 12 \times 12$ Monkhorst–Pack $\boldsymbol{k}$-grid [46]. The structures were relaxed using the conjugate gradient technique with the energy convergence criteria set at 10^{-8} eV and 10^{-6} eV for the electronic and ionic iterations, respectively. The symmetry of the structures was analyzed with the FINDSYM [47] and SeeK-path [48, 49] packages.

Using the results of DFT calculation for the electronic band structure, we can find a tight binding model in the basis of the maximally localized Wannier orbitals [50–52]. This can be performed via the Wannier90 software [53–55]. In our calculations, we used the $10 \times 10 \times 10$ full $\boldsymbol{k}$-point DFT calculation, starting from the p orbitals for Pb atoms, the p and d orbitals for Pd atoms. This gives us a 28-orbital tight-binding model of Pb_2Pd. Finally, to study the surface states, the surface Green's function for the semi-infinite system [56] was calculated using WannierTools [57].

2.2. Crystal structure

Pb_2Pd crystallizes with the $I4/mcm$ symmetry (space group No. 140), i.e., a body-centered tetragonal unit cell with Pd atoms at the body center (see Fig. 1a). After optimizing DFT, the lattice constants were found to be $a = b = 6.997$ Å, and $c = 5.920$ Å, which are close to the experimentally reported values $a = b = 6.863$ Å, and $c = 5.840$ Å [29]. The Pd and Pb atoms are located in the high symmetry Wyckoff positions $4a$ $(0, 0, 0.25)$, and $8h$ $(0.1630, 0.6630, 0)$, respectively. Here, it should be noted that the Pb atom position obtained experimentally was $(0.1643, 0.6643, 0)$, which is close to the theoretical one [29].

2.3. Bulk electronic band structure

The bulk electronic band structure is presented in Fig. 2 (orange and blue lines correspond to the results of the absence and presence of spin–orbit coupling, respectively). Several nearly-flat bands (approximately 2 eV below the Fermi level) can be distinguished in the band structure. However, around the Fermi level, the bands exhibit strong dispersion.

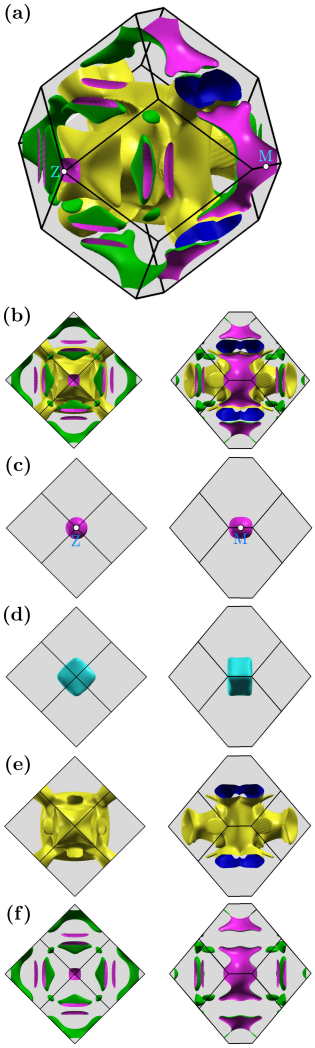

Fig. 3. The Fermi surface of Pb_2Pd with $I4/mcm$ symmetry in the presence of spin–orbit coupling. Panels (a) and (b) present the full Fermi surface, while panels (c)–(f) present separate pockets.

The introduction of spin–orbit coupling causes the splitting of electronic bands. This is clearly visible, e.g., at the Γ point, where the splitting is in the range of 0.5 eV. However, the largest impact of spin–orbit coupling on the band structure is visible mainly above the Fermi level — e.g., at the M point, around 2 eV above the Fermi level, where a strong modification of the band structure is observed.

The four bands forming the Fermi surface (Fig. 3) have an electronic character. The first two bands, with a nearly parabolic-like dispersion relation around the Γ point, create two sphere-like pockets (Fig. 3c and d). The next two bands show a strong $\boldsymbol{k}$-dependence (Fig. 3e and f).

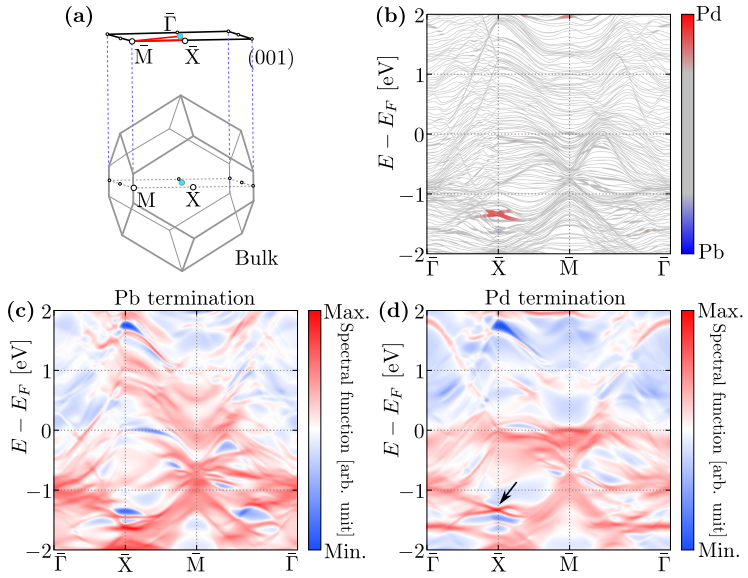

Fig. 4. (a) Projection of the bulk Brillouin zone on the (001) surface of the Brillouin zone. (b) Electronic band structure from the slab-type calculation. The color corresponds to the contribution of the surface with a different type of termination (as marked in the legend). In panels (c) and (d), the surface spectral function for different surface terminations are presented (see the legend).

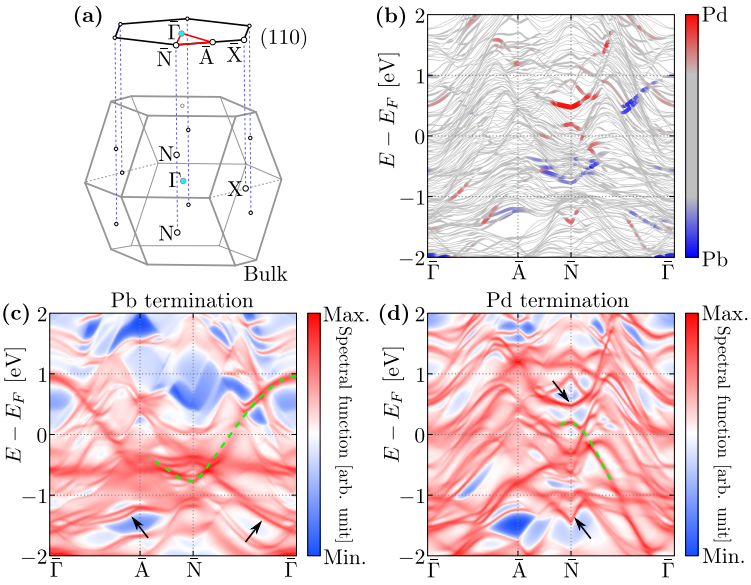

Fig. 5. (a) Projection of the bulk Brillouin zone on the (110) surface of the Brillouin zone. (b) Electronic band structure from the slab-type calculation. The color corresponds to the contribution of the surface with a different type of termination (as marked in the legend). In panels (c) and (d), the surface spectral function for different surface terminations are presented (see the legend).

2.4. Surface states

Now, we will present analyses of surface states for surfaces (001) and (110) (respectively, Fig. 4 and Fig. 5), which host surface states in close vicinity of the Fermi level.

The electronic band structure calculated for the slab geometry (panel (b)) presents a very complex structure (blue to the projection of the 3D bulk Brillouin zone to the 2D surface Brillouin zone, shown in panel (a)). The absence of periodic boundary conditions along the direction parallel to the surface allows the realization of the surface states as a consequence of dangling bonds of atoms on the surface. Indeed, direct analyses of the band projection on the surface atoms reflect the presence of surface states (color contours on panel (b)). The realized geometry allows us to find surface states realized by a surface terminated by the Pb atoms (blue), as well as by the Pd atoms (red). As we can see, in

the case of the (001) surface (Fig. 4b), the Dirac cone-like structure at the $\bar{X}$ point is clearly visible. In the presented range of energies around the Fermi level, we do not observe any surface states coming from the Pb terminated surface. Contrary to this, for surface (110), both terminated surfaces allow the realization of surface states. Here we can distinguish several surface states in close vicinity of the Fermi level (from both types of terminations).

We also calculate the surface Green's function (spectral function) for the semi-infinite system with Pb and Pd termination (panels (c) and (d) in Fig. 4 and Fig. 5, respectively). In the case of the Pb terminated (110) surface, the surface state forms a parabolic-like band crossing the Fermi level (marked with the green dashed line in Fig. 5c). However, also at deeper energies, the surface states are visible as separate sharp lines with high spectral weights (marked with black arrows around -1.5 eV in Fig. 5c).

In the case of the Pd termination of (001) surface, the earlier-mentioned Dirac cone-like structures are also clearly visible in the spectral function (marked with black arrows in Fig. 5d). For surface (110), surface states coming from Pd termination are more visible for several energies at the $\bar{N}$ point. First, the parabolic-like surface states crossing the Fermi level can clearly be seen. Moreover, two separated surface states at 0.5 eV and -1.25 eV are also visible (marked with the black arrows in Fig. 5d).

As we mentioned above, in the case of the (110) surface, parabolic-like surface states are clearly visible in the spectrum. Here it is worth mentioning that these parabolic dispersion relations have a different character for Pb termination (electron-like) and for Pd termination (hole-like).

3. Conclusions

In summary, we discussed surface states realized in Pb_2Pd, for surfaces (001) and (110) terminated by Pb or Pd atoms. As a consequence of the dangling bonds of the atoms at the surface, electronic surface states can be realized. We calculate surface Green's (spectral) functions for the mentioned surfaces. In the case of (001) surface, the Dirac cone surface states at the $\bar{X}$ point can be observed. However, this surface state is located deep down the Fermi surface and should not play an important role in the physical properties of Pb_2Pd. Contrary to this, for (110) surface, surface states can be realized for both terminations of the surface. Additionally, surface states around the $\bar{N}$ point exist in close vicinity of the Fermi surface. Moreover, these states exhibit a parabolic-like relation with different (electron- or hole-like) character. In our opinion, such states should be experimentally observed in a relatively simple way within the ARPES measurements.

Acknowledgments

Some figures in this work were rendered using VESTA [58] and XCrySDen [59] software. S.B. is grateful to IT4Innovations (VSB-TU Ostrava) for hospitality during a part of the work on this project. This work was supported by the National Science Centre (NCN, Poland) under grants Nos. 2017/25/B/ST3/02586 (S.B.) and 2021/43/B/ST3/02166 (A.P.). A.P. appreciates funding in the frame of scholarships of the Minister of Science and Higher Education (Poland) for outstanding young scientists (2019 edition, No. 818/STYP/14/2019).

References

[1] M.Z. Hasan, C.L. Kane, *Rev. Mod. Phys.* **82**, 3045 (2010).

[2] X.-L. Qi, S.-Ch. Zhang, *Rev. Mod. Phys.* **83**, 1057 (2011).

[3] H. Zhang, Ch.-X. Liu, X.-L. Qi, X. Dai, Z. Fang, S.-Ch. Zhang, *Nat. Phys.* **5**, 438 (2009).

[4] Y. Xia, D. Qian, D. Hsieh et al., *Nat. Phys.* **5**, 398 (2009).

[5] Y.L. Chen, J.G. Analytis, J.-H. Chu et al., *Science* **325**, 178 (2009).

[6] Y.L. Chen, J.-H. Chu, J.G. Analytis et al., *Science* **329**, 659 (2010).

[7] S.-Y. Xu, M. Neupane, Ch. Liu et al., *Nature Physics* **8**, 616 (2012).

[8] A. Ptok, K.J. Kapcia, A. Ciechan, *J. Phys.: Condens. Matter* **33**, 065501 (2020).

[9] M.M. Otrokov, I.I. Klimovskikh, H. Bentmann et al., *Nature* **576**, 416 (2019).

[10] Y. Gong, J. Guo, J. Li et al., *Chinese Phys. Lett.* **36**, 076801 (2019).

[11] J.-Q. Yan, Q. Zhang, T. Heitmann et al., *Phys. Rev. Materials* **3**, 064202 (2019).

[12] P. Swatek, Y. Wu, L.-L. Wang, K. Lee, B. Schrunk, J. Yan, A. Kaminski, *Phys. Rev. B* **101**, 161109 (2020).

[13] S.M. Young, S. Zaheer, J.C.Y. Teo, C.L. Kane, E.J. Mele, A.M. Rappe, *Phys. Rev. Lett.* **108**, 140405 (2012).

[14] Z.K. Liu, B. Zhou, Y. Zhang et al., *Science* **343**, 864 (2014).

[15] L.M. Schoop, A. Topp, J. Lippmann et al., *Sci. Adv.* **4**, eaar2317 (2018).

[16] S.-Y. Xu, I. Belopolski, N. Alidoust et al., *Science* **349**, 613 (2015).

[17] H. Weng, Ch. Fang, Z. Fang, B.A. Bernevig, X. Dai, *Phys. Rev. X* **5**, 011029 (2015).

[18] B.Q. Lv, H.M. Weng, B.B. Fu et al., *Phys. Rev. X* **5**, 031013 (2015).

[19] Z. Wang, M.G. Vergniory, S. Kushwaha, M. Hirschberger, E.V. Chulkov, A. Ernst, N.P. Ong, R.J. Cava, B.A. Bernevig, *Phys. Rev. Lett.* **117**, 236401 (2016).

[20] R. Yu, Q. Wu, Z. Fang, H. Weng, *Phys. Rev. Lett.* **119**, 036401 (2017).

[21] Ch. Fang, H. Weng, X. Dai, Z. Fang, *Chinese Phys. B* **25**, 117106 (2016).

[22] L.M. Schoop, M.N. Ali, C. Straßer, A. Topp, A. Varykhalov, D. Marchenko, V. Duppel, S.S.P. Parkin, B.V. Lotsch, C.R. Ast, *Nature Communications* **7**, 11696 (2016).

[23] D. Takane, Z. Wang, S. Souma, K. Nakayama, C.X. Trang, T. Sato, T. Takahashi, Yoichi Ando, *Phys. Rev. B* **94**, 121108 (2016).

[24] C. Chen, X. Xu, J. Jiang et al., *Phys. Rev. B* **95**, 125126 (2017).

[25] M.M. Hosen, K. Dimitri, I. Belopolski et al., *Phys. Rev. B* **95**, 161101 (2017).

[26] R. Wang, J.Z. Zhao, Y.J. Jin, Y.P. Du, Y.X. Zhao, H. Xu, S.Y. Tong, *Phys. Rev. B* **97**, 241111 (2018).

[27] B.-B. Fu, C.-J. Yi, T.-T. Zhang et al., *Sci. Adv.* **5**, eaau6459 (2019).

[28] M.F. Gendron, R.E. Jones, *J. Phys. Chem. Solids* **23**, 405 (1962).

[29] M.M. Sharma, N.K. Karn, P. Rani, R.N. Bhowmik, V.P.S. Awana, *Supercond. Sci. Technol.* **35**, 084010 (2022).

[30] M. Wang, K. Tang, *Phys. C* **565**, 1353518 (2019).

[31] H. Leng, J.-C. Orain, A. Amato, Y.K. Huang, A. de Visser, *Phys. Rev. B* **100**, 224501 (2019).

[32] Arushi, K. Motla, A. Kataria, S. Sharma, J. Beare, M. Pula, M. Nugent, G.M. Luke, R.P. Singh, *Phys. Rev. B* **103**, 184506 (2021).

[33] F. Martín-Vega, E. Herrera, B. Wu et al., *Phys. Rev. Research* **4**, 023241 (2022).

[34] N. Kumar, M. Yao, J. Nayak et al., *Adv. Mater.* **32**, 1906046 (2020).

[35] Y. Liu, J.-Z. Zhao, L. Yu et al., *Chinese Phys. Lett.* **32**, 067303 (2015).

[36] F. Fei, X. Bo, R. Wang, B. Wu, J. Jiang, D. Fu, M. Gao, H. Zheng, Y. Chen, X. Wang, H. Bu, F. Song, X. Wan, B. Wang, G. Wang, *Phys. Rev. B* **96**, 041201 (2017).

[37] H.-J. Noh, J. Jeong, E.-J. Cho, K. Kim, B.I. Min, B.-G. Park, *Phys. Rev. Lett.* **119**, 016401 (2017).

[38] M.S. Bahramy, O.J. Clark, B.-J. Yanget al., *Nat. Mater.* **17**, 28 (2018).

[39] K. Iwaya, Y. Kohsaka, K. Okawa, T. Machida, M.S. Bahramy, T. Hanaguri, T. Sasagawa, *Nat. Commun.* **8**, 976 (2017).

[40] Peng-Fei Liu, Jingyu Li, Xin-Hai Tu, Huabing Yin, Baisheng Sa, Junrong Zhang, D.J. Singh, Bao-Tian Wang, *Phys. Rev. B* **102**, 155406 (2020).

[41] P.E. Blöchl, *Phys. Rev. B* **50**, 17953 (1994).

[42] G. Kresse, J. Hafner, *Phys. Rev. B* **49**, 14251 (1994).

[43] G. Kresse, J. Furthmüller, *Phys. Rev. B* **54**, 11169 (1996).

[44] G. Kresse, D. Joubert, *Phys. Rev. B* **59**, 1758 (1999).

[45] J.P. Perdew, K. Burke, M. Ernzerhof, *Phys. Rev. Lett.* **77**, 3865 (1996).

[46] H.J. Monkhorst, J.D. Pack, *Phys. Rev. B* **13**, 5188 (1976).

[47] H.T. Stokes, D.M. Hatch, *J. Appl. Crystallogr.* **38**, 237 (2005).

[48] Y. Hinuma, G. Pizzi, Y. Kumagai, F. Oba, I. Tanaka, *Comput. Mater. Sci.* **128**, 140 (2017).

[49] A. Togo, I. Tanaka, arXiv:1808.01590 (2018).

[50] N. Marzari, A.A. Mostofi, J.R. Yates, I. Souza, D. Vanderbilt, *Rev. Mod. Phys.* **84**, 1419 (2012).

[51] N. Marzari, D. Vanderbilt, *Phys. Rev. B* **56**, 12847 (1997).

[52] I. Souza, N. Marzari, D. Vanderbilt, *Phys. Rev. B* **65**, 035109 (2001).

[53] A.A. Mostofi, J.R. Yates, Y.-S. Lee, I. Souza, D. Vanderbilt, N. Marzari, *Comput. Phys. Commun.* **178**, 685 (2008).

[54] A.A. Mostofi, J.R. Yates, G. Pizzi, Y.-S. Lee, I. Souza, D. Vanderbilt, N. Marzari, *Comput. Phys. Commun.* **185**, 2309 (2014).

[55] G. Pizzi, V. Vitale, R. Arita et al., *J. Phys.: Condens. Matter* **32**, 165902 (2020).

[56] M.P. Lopez Sancho, J.M. Lopez Sancho, J.M.L. Sancho, J. Rubio, *J. Phys. F: Met. Phys.* **15**, 851 (1985).

[57] Q.S. Wu, S.N. Zhang, H.-F. Song, M. Troyer, A.A. Soluyanov, *Comput. Phys. Commun.* **224**, 405 (2018).

[58] K. Momma, F. Izumi, *J. Appl. Crystallogr.***44**, 1272 (2011).

[59] A. Kokalj, *J. Mol. Graph. and Model.* **17**, 176 (1999).